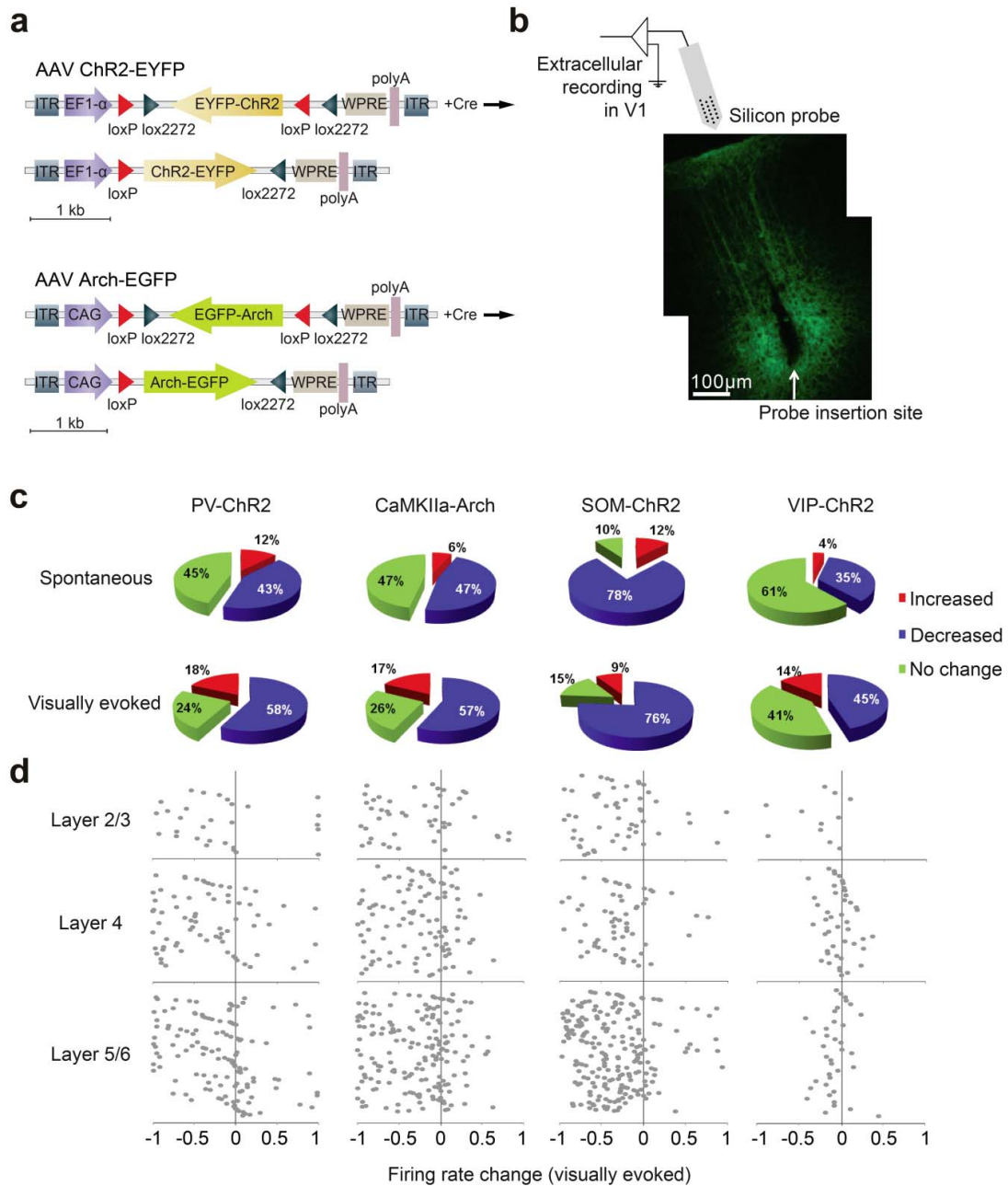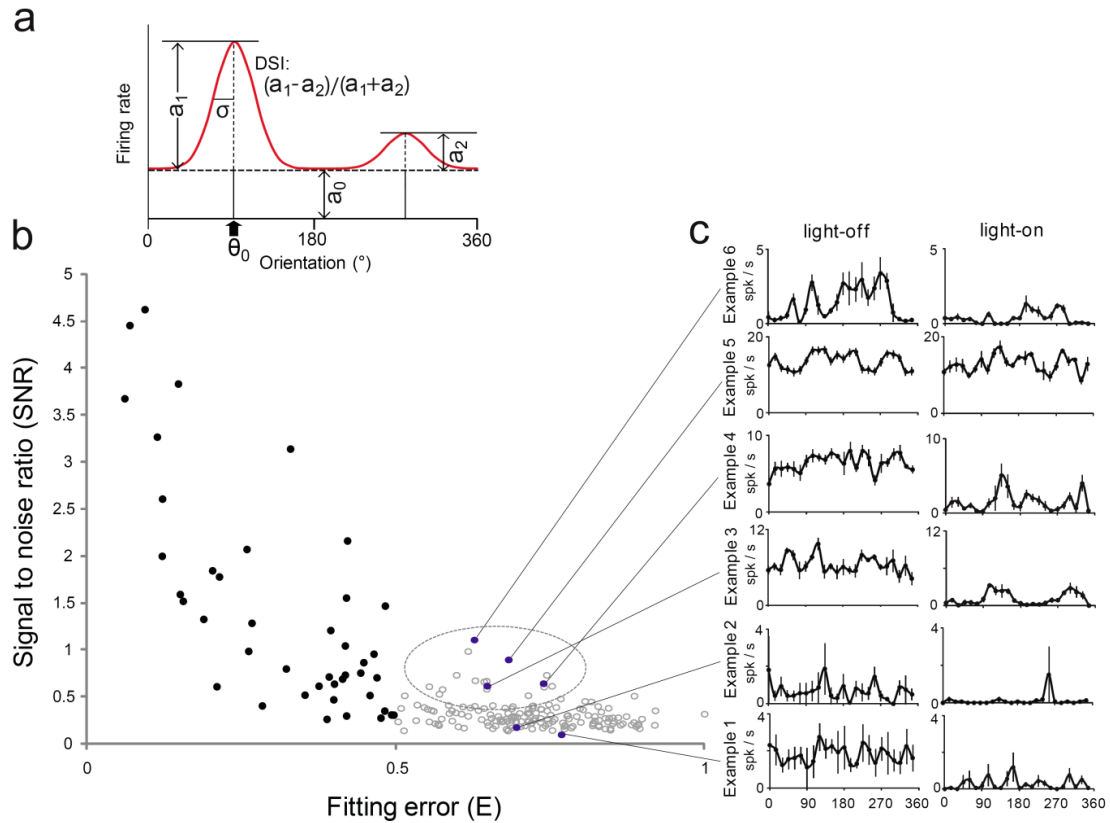## Supplementary Figures and Legends
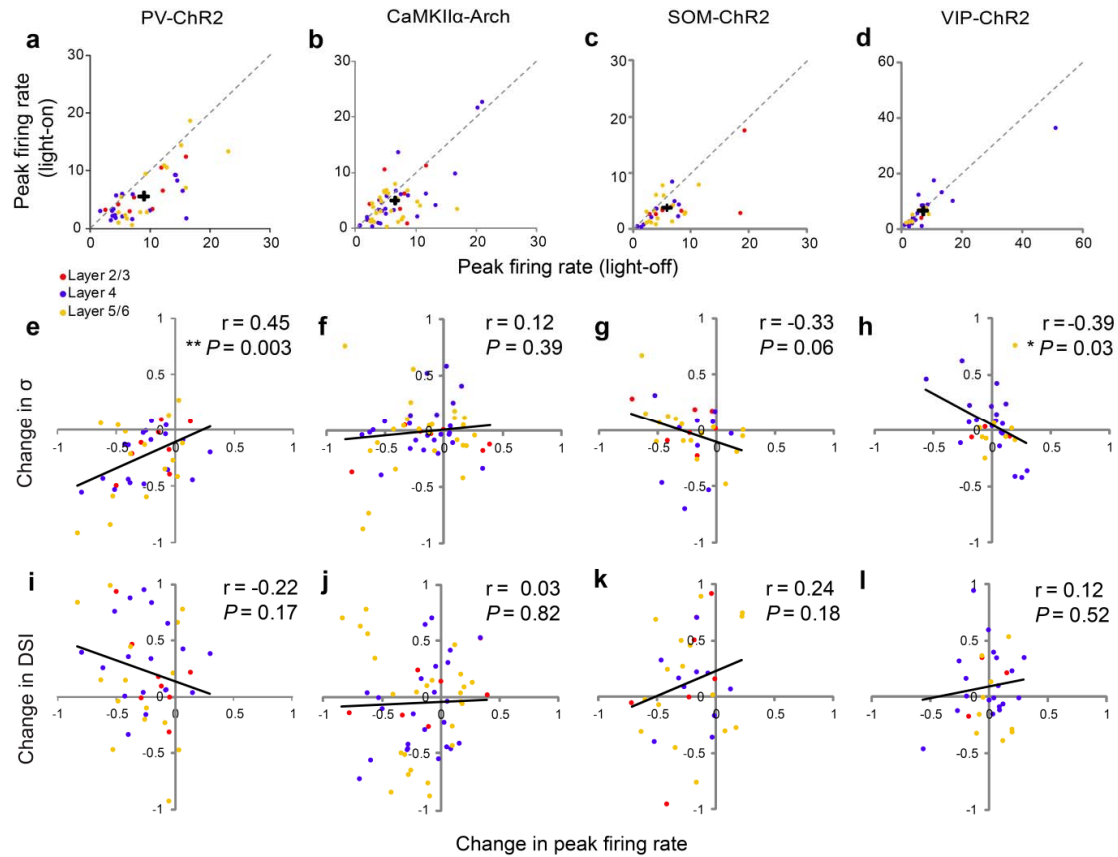

Supplementary Figure 1 | Changes in firing rate induced by laser stimulation in different cortical layers in anesthetized mouse V1. **a,** Schematics for the viral vectors used for cell-type specific expression of ChR2 and Arch. **b**, Fluorescence image showing the insertion site of the silicon probe in V1 injected with the viral vector. Image was from a CaMKIIα-ChR2-EYFP mouse. **c**, Fractions of neurons showing significant increase ($P < 0.01$, bootstrap), significant decrease, and no significant change in spontaneous (upper row) and
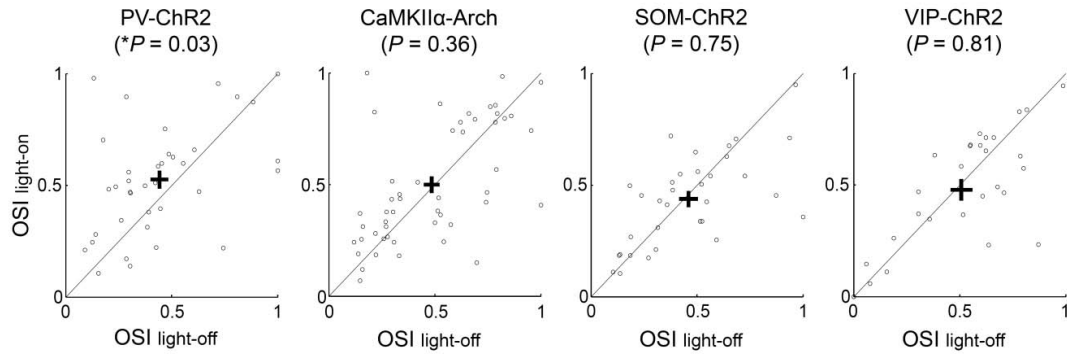
visually evoked (lower row) firing rates upon laser stimulation, in PV-ChR2, CaMKIIα-Arch, SOM-ChR2, and VIP-ChR2 mice. **d**, Changes in visually evoked firing rate in different cortical layers induced by ChR2-mediated activation of different types of inhibitory interneurons or Arch-mediated silencing of excitatory neurons, measured by ($R_{light-on}$ - $R_{light-off}$)/($R_{light-on}$ + $R_{light-off}$), where $R_{light-on}$ and $R_{light-off}$ are firing rates during laser on and off periods, respectively, averaged across all orientations. Each symbol represents one single unit. The layers were identified based on the recording depth (layer 2/3, 100 μm - 350 μm; layer 4, 350 μm - 500 μm; layer 5/6, 500 μm - 1 mm) as well as multiunit activity in response to a transient visual stimulus (layers 4 and 6 showed short latencies of 40 to 50 ms, and layer 2/3 and 5 showed delayed responses at 70 to 100 ms).
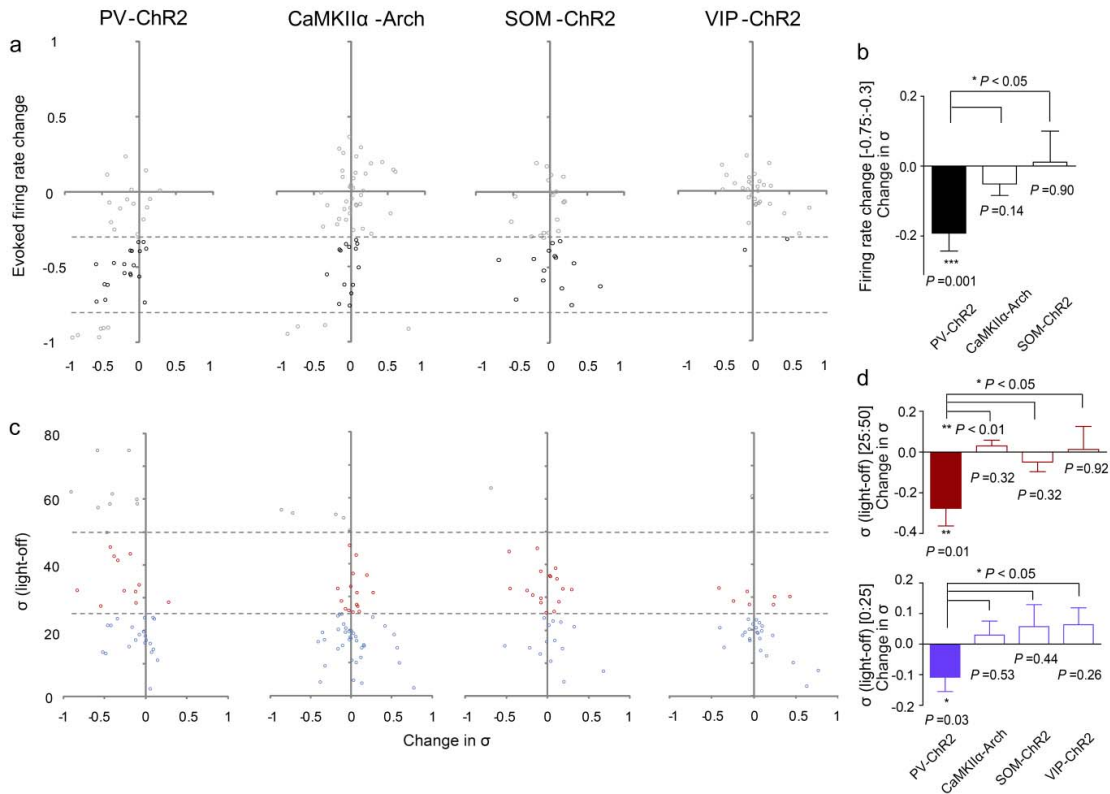
Supplementary Figure 2 | Quantification of orientation tuning and direction selectivity by fitting with a double Gaussian function. **a**, Schematic illustration of the parameters of the double Gaussian function. **b**, Scatter plot of signal-to-noise ratio (SNR) of the tuning curve vs. fitting error (E) in the PV-ChR2 group. Each symbol represents one cell. Black filled dots, cells with E < 0.5, included in the quantitative analysis of σ and DSI. Gray open circles, cells with E > 0.5, excluded from the quantitative analysis. Blue filled dots, cells whose tuning curves are shown in **c**. Dotted ellipse, cells with E > 0.5, but relatively high SNR. **c**. Six example cells (blue filled dots in **b**).
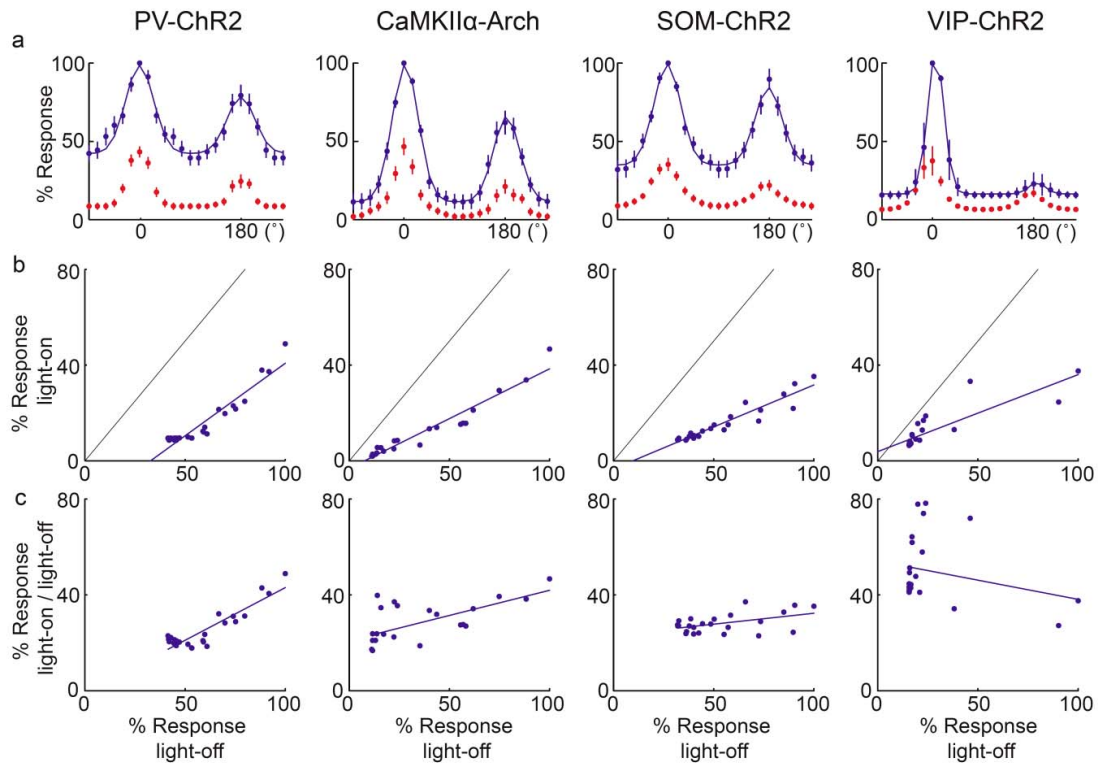
Supplementary Figure 3 | Laser-induced changes in peak firing rate and stimulus selectivity measured in PV-ChR2, CaMKIIα-Arch, SOM-ChR2, and VIP-ChR2 mice. a-d, peak firing rate (firing rate at the preferred orientation and direction) with laser on vs. laser off. Each dot represents one cell. Layers are represented by colors. Cross, population average (± s.e.m.). **e-h**, Change in σ (measured by $(\sigma_{light\text{-}on} - \sigma_{light\text{-}off})/(\sigma_{light\text{-}on} + \sigma_{light\text{-}off})$) vs. peak firing rate change. **i-l**, Change in DSI (measured by $(DSI_{light\text{-}on} - DSI_{light\text{-}off})/(DSI_{light\text{-}on} + DSI_{light\text{-}off})$) vs. peak firing rate change. Circle, individual cell. Line, linear regression for the population.
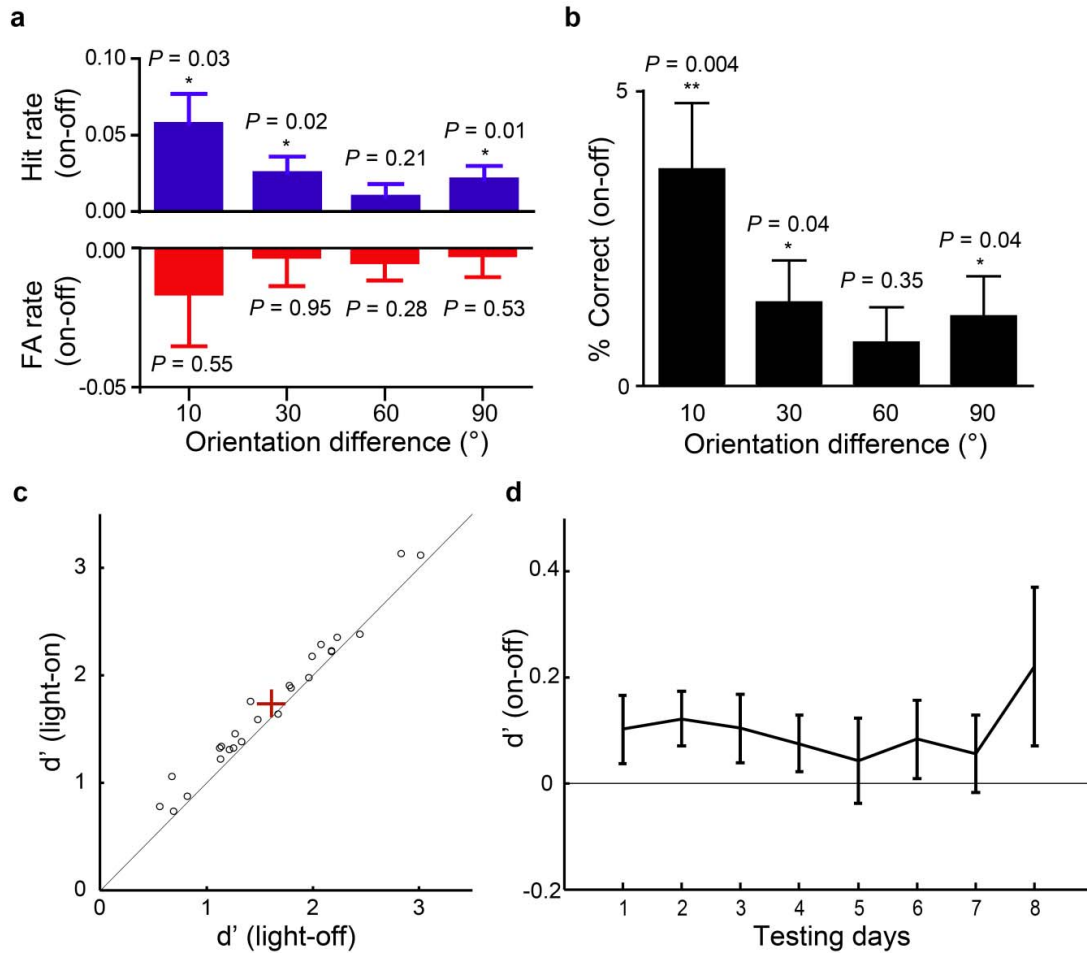
Supplementary Figure 4 | Laser-induced changes in orientation selectivity index in PV-ChR2, CaMKIIα-Arch, SOM-ChR2, and VIP-ChR2 mice. Orientation selectivity index (OSI) was calculated as 1 - circular variance[23]. Laser stimulation caused a significant increase in OSI in PV-ChR2 mice but not in CaMKIIα-Arch, SOM-ChR2, or VIP-ChR2 mice (paired *t*-test).

Supplementary Figure 5 | Comparison of laser-induced changes in σ across groups with matching firing rate change and σ (light-off). a, Scatter plot of evoked firing rate change (laser induced change in visually evoked firing rate, averaged across all orientations) vs. change in σ, for the four groups of cells. Each symbol represents one cell. Dashed lines delineate the range of firing rate change [-0.75 -0.3] within which the four groups were compared. Note that except for the VIP-ChR2 group, the firing rate change was well matched among the other three groups within this range. **b**, Laser-induced change in σ for cells within the range indicated in **a** in each group, mean ± s.e.m. The VIP-ChR2 group was omitted since there were only two cells in the range. The reduction was significant in the PV-ChR2 (solid bar) but not in CaMKIIα-Arch and SOM-ChR2 groups (open bars), *P* value below each bar indicates significance of the change within each group. The difference between the PV-ChR2 and each of the other two groups was significant (*P* value on top of plot). **c**, Scatter plot of σ (light-off) vs. change in σ, for the four groups of cells. Dashed lines delineate the two ranges of σ (light-off), broad ([25° 50°], red) and narrow ([0° 25°], blue), within which the four groups were compared. **d**, Laser-induced change in σ for cells within the broad (upper) and narrow (lower) ranges in each group, mean ± s.e.m. The reduction was significant in the PV-ChR2 (solid bar) but not in the CaMKIIα-Arch, SOM-ChR2 and VIP-ChR2 (open bar) groups, and the difference between PV-ChR2 and each of the other three groups was significant.
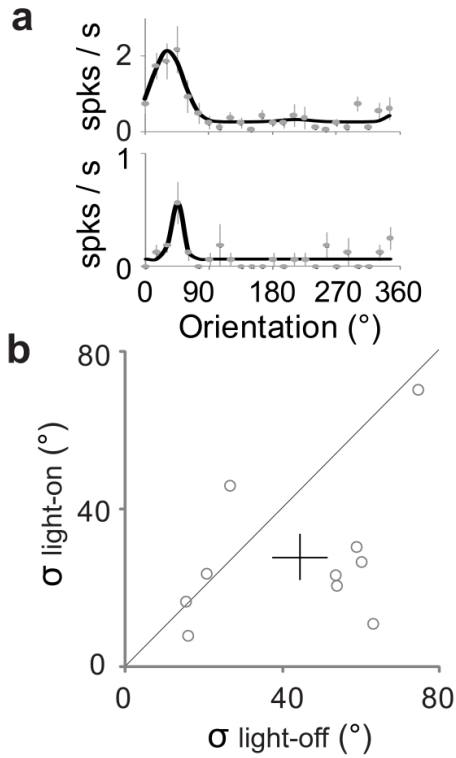
Supplementary Figure 6 | Effects of laser on firing rates at different stimulus directions for neurons in PV-ChR2, CaMKIIα-Arch, SOM-ChR2 and VIP-ChR2 groups whose firing rate changes fall between -0.75 and -0.3 (between dashed lines in Supplementary Fig. 5a). a, Median response of the neurons to 24 directions with (red) or without (blue) laser stimulation. The median response was computed after aligning the tuning curves of all cells in each group to the same preferred orientation (0°). Blue line: fit with double Gaussian function to the response without laser stimulation. **b**, Median responses to 24 directions with laser stimulation plotted against those without laser. Line, linear fit to data (PV-ChR2, slope 0.61, horizontal offset 32.7%; CaMKIIα-Arch, slope 0.42, offset 7.6%; SOM-ChR2, slope 0.35, offset 9.5%; VIP-ChR2, slope 0.32, offset -12.1%). The plots in **a** and **b** are analogous to Fig. 4A,B in the study of Atallah et al[23]. **c**, Amount of laser-induced suppression vs. response without laser at each stimulus direction. Line, linear fit to data (slope: PV-ChR2, 0.44; CaMKIIα-Arch, 0.21; SOM-ChR2, 0.09; VIP-ChR2, -0.16). Note that among the four groups PV-ChR2 shows the strongest correlation between the degree of suppression and the response without laser. Stronger suppression of the responses at non-preferred orientations caused sharpening of tuning.

Supplementary Figure 7 | Effects of PV+ neuron activation on orientation discrimination. **a**, Effect of laser on hit and false alarm rates at each of the four Δθ values, measured by the difference between the laser on and laser off trials for each mouse, averaged across all mice (n = 9 to 25). Error bar, ± s.e.m. *P* value on top of each bar indicates significance of the effect of laser stimulation at each orientation difference. **b**, Laser-induced change in % of correct trials. **c**, d' of each mouse (combined across all Δθ values and all test sessions) during laser on vs. laser off. The difference between light-on and light-off was significant ($P = 4 \times 10^{-5}$, Wilcoxon signed rank test, n = 25). **d**, Effect of laser stimulation on d' over multiple days of testing. For each mouse the data at all Δθ values were combined. Error bar, ± s.e.m.

PV-ChR2: Awake

Supplementary Figure 8 | Effect of laser stimulation on orientation tuning in awake PV-ChR2 mice. **a**, Example tuning curves. **b,** σ with and without laser stimulation (light-off, 44.2 ± 7.0°, light-on, 27.9 ± 5.8°, mean ± s.e.m., n = 10; $P < 0.05$, paired t-test).